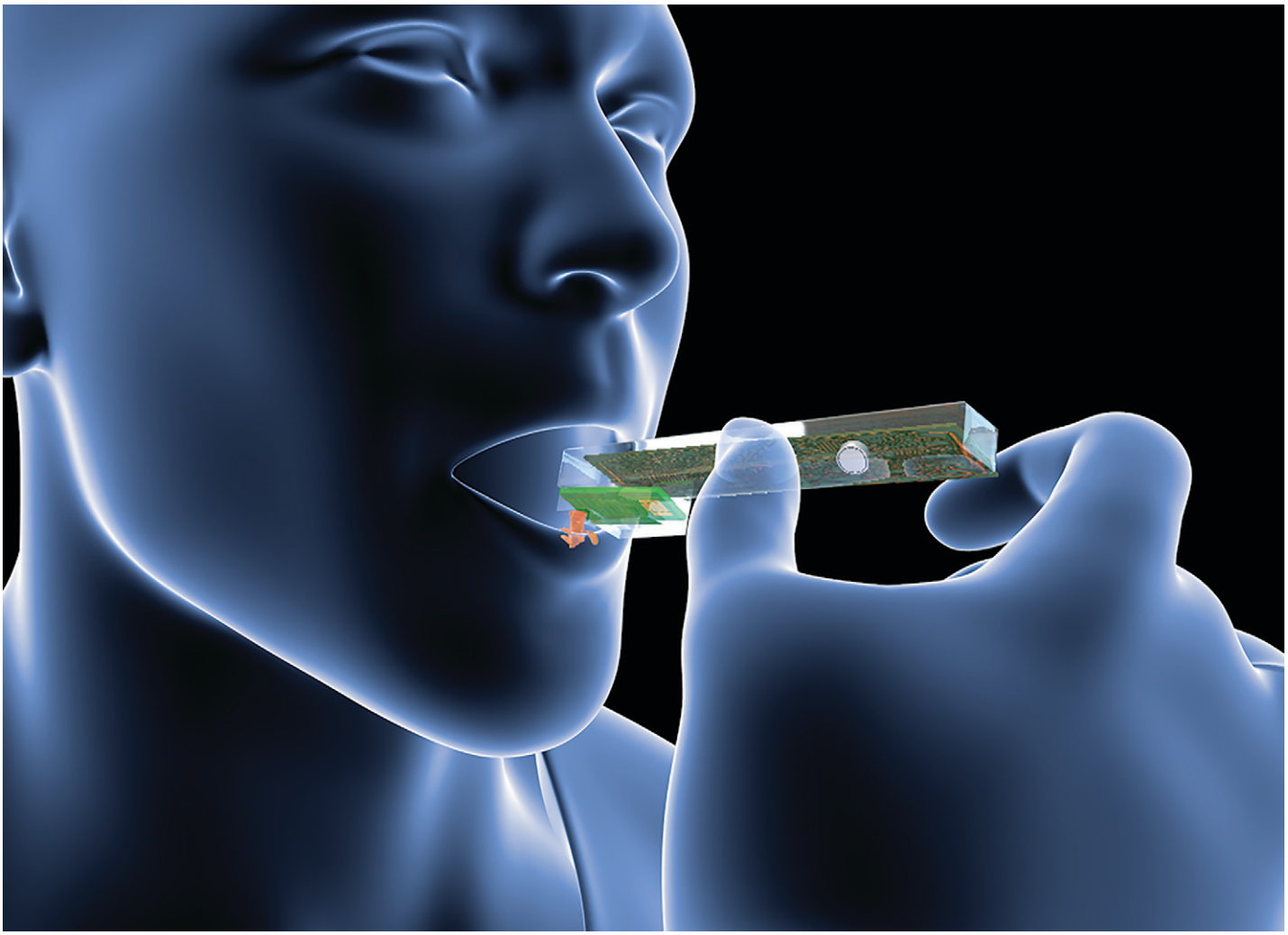

Featuring work from the Micro/Nanophysics Research Laboratory of Professor Leslie Yeo, RMIT University, Australia.

High frequency acoustic permeabilisation of drugs through tissue for localised mucosal delivery

Using a miniature handheld and portable microacoustofluidic device, drugs can be efficiently localised within the mucosal layer without penetrating deeper into the systemic circulation, thus allowing a rapid and effective means for vaccination.

As featured in:

See Leslie Y. Yeo *et al.*, *Lab Chip*, 2018, **18**, 3272.

ROYAL SOCIETY OF CHEMISTRY

rsc.li/loc

Registered charity number: 207890

Lab on a Chip

PAPER

View Article Online
View Journal | View Issue

Cite this: *Lab Chip*, 2018, **18**, 3272

High frequency acoustic permeabilisation of drugs through tissue for localised mucosal delivery

Shwathy Ramesan, Amgad R. Rezk and Leslie Y. Yeo *

Received 5th April 2018,
Accepted 13th September 2018

DOI: 10.1039/c8lc00355f

rsc.li/loc

The majority of infectious diseases enter the body through mucosal membranes that line the ocular, nasal, oral, vaginal and rectal surfaces. As infections can be effectively prevented by instigating a local immune response in the immunocyte-rich regions of the mucosa, an efficacious route of vaccine administration is to directly target their delivery to these surfaces. It is nevertheless challenging to provide sufficient driving force to penetrate both the mucus lining as well as the epithelial barrier of the mucosal surfaces, which are designed to effectively keep foreign entities out, but not excessively such that the therapeutic agent penetrates deeper into the vascularised submucosal regions where they are mostly taken up by the systemic circulation, thus resulting in a far weaker immune response. In this work, we demonstrate the possibility of controllably localising and hence maximising the delivery of both small and large molecule model therapeutic agents in the mucosa of a porcine buccal model using high frequency acoustics. Unlike their low (kHz order) frequency bulk ultrasonic counterpart, these high frequency (>10 MHz) surface waves do not generate cavitation, which leads to large molecular penetration depths beyond the 100 μm order thick mucosal layer, and which has been known to cause considerable cellular/tissue damage and hence scarring. Through system parameters such as the acoustic irradiation frequency, power and exposure duration, we show that it is possible to tune the penetration depth such that over 95% of the delivered drug are localised within the mucosal layer, whilst preserving their structural integrity.

1 Introduction

The vast surface area of the mucosal membranes that line the respiratory, digestive and reproductive tracts—over several hundred square meters in an adult body, and much greater than that of skin—and their constant exposure to the external environment or food makes them particularly susceptible as an entry portal for over 70% of infectious agents into the body.[1] As the first line of defence, over 80% of all immunocytes in the human body are thus present in mucosa-associated lymphoid tissue (MALT).[2] The abundance of these innate and adaptive immune system cells in the MALT, including phagocytic neutrophils and macrophages, monocytes, natural killer cells, dendritic cells and other antigen-presenting cells that recognise and respond to antigenic challenges, produce pathogen-specific antibodies that are secreted into the mucus where they are able to neutralise the threat before an infection occurs.[3–7]

For this reason, the mucosa is an attractive target for local vaccine delivery to elicit a far stronger local immune response than that possible *via* systemic vaccination routes such as subcutaneous or intramuscular injection.[8,9] In any case, the vascularised nature of the mucosal surfaces also facilitates the induction of systemic immunity.[7] Another advantage of mucosal delivery is that it comprises a non-invasive needle-free route, which is attractive particularly for vaccination in developing nations and among children.

There are, however, considerable hurdles that underscore the difficulties of effective mucosal delivery. For one, the mucosa is designed with a robust tolerance mechanism that regulates the immune response to prevent antigenic overreaction.[9] Further, the mucus that coats all mucosal surfaces is endowed with natural defence mechanisms designed as a barrier to prevent entry. In addition to the bulk motion of the mucus that impedes deposition and hence facilitates rapid removal, substances that find their way to the mucosal epithelium are trapped by the heterogenous viscous and sticky mucus layer where they are degraded by its acid- or enzyme-rich environment.

In addition to the design of mucosal vaccines and the use of appropriate adjuvants to safely increase immunogenicity, various strategies have therefore been proposed to increase penetration of therapeutic agents through the mucus by circumventing the physiological barriers to diffusional transport along the mucosal route, such as the hydrophobic and electrostatic interactions that lead to aggregation in the mucus microstructure.[10] These strategies have, however,

Micro/Nanophysics Research Laboratory, RMIT University, Melbourne, VIC 3000, Australia. E-mail: leslie.yeo@rmit.edu.au

primarily focussed on appropriate choice of viral and synthetic drug carriers and modifying their surfaces to alter mucoadhesion and increase mucus penetration.[7,11,12] Alternatively, it is possible to improve drug penetration either by physically disrupting the mucus layer through the use of mucolytic agents[13,14] or by enhancing permeabilisation of the mucosal membrane, for example, sonophoretically by employing ultrasound.[15,16] Compared to the focus on the use of biochemical carriers, physical membrane disruption methods, nevertheless, remain relatively unexplored.

On the one hand, ultrasound has long been employed as a method for physical membrane disruption to enhance entry of drugs to cells. The majority of work has however predominantly been carried out at low (10 kHz order) frequencies.[15] This is because cavitational effects—which not only leads to the removal of lipids in the intercellular domains, particularly in the stratum corneum such that its permeabilisation to drugs is enhanced, but also provides the large pressures necessary to drive the drug sonophoretically through tissue—decreases exponentially with increasing frequencies.[17,18] While ultrasonic delivery *via* cavitation at low frequency thus facilitates effective transdermal delivery where it is necessary for the therapeutic agent to penetrate deeply to depths of approximately 1 mm beneath the skin's outer layer into the highly vascularised dermis layer for absorption into the systemic circulation,[19] such depths are excessive for localising the drug within the mucosal epithelium for optimal mucosal delivery.

As it is the viable epidermis that assumes the rate limiting step and hence barrier for efficient molecular transport following permeabilisation of the stratum corneum,[20] we therefore believe that it is more expedient to exploit the far shorter attenuation lengths associated with higher frequency sound waves above 10 MHz, where cavitation is also essentially non-existent,[21,22] to confine drug transport within the mucosal layer, which typically possesses thicknesses in the range 100–200 μm in the sublingual regions, 200–500 μm in the ocular regions, 500–800 μm in the buccal regions, 660–1130 μm in the rectal regions,[23] and 1.3–1.4 mm in the vaginal regions.[9,24,25] By doing so, the vaccine antigen that is delivered to either of these routes does not enter the bloodstream *via* the capillary-rich regions of the submucosa at distances beyond the mucosal layer thicknesses, but are captured by the antigen-presenting cells in the mucosa to elicit an effective local mucosal immune response. Given that large cavitational stresses also lead to considerable damage to cells and tissues as a result of the poration of the cell membrane (the very mechanism responsible for the efficient intercellular permeabilisation of the drug during sonoporation drug delivery), another advantage of suppressing cavitation with high frequency excitation is the considerably lower cell/tissue damage and scarring.

In this work, we hence show that it is possible to achieve localisation of model therapeutic agents within the mucosal layer of a porcine lip, given its close resemblance to the human buccal mucosa, through the use of a particular form of high frequency (10 MHz order) sound waves, namely, surface acoustic waves (SAWs). SAWs have recently been demonstrated for a host of microfluidic applications[22,26–28] including particle/cell patterning, sorting and alignment,[29–33] sessile and microchannel droplet transport and manipulation,[34–41] microchannel/nanochannel actuation,[42–49] microcentrifugation,[50–56] jetting,[57] and nebulisation.[58–64] Other than as an aerosol generator for inhaled therapeutics *via* the nebulisation process,[65–68] and, more recently, as a vibration source that enhances cytosolic intracellular delivery without necessitating pore formation,[69] SAWs have however yet to be exploited for other administrative modes of drug delivery, let alone that through tissue and specifically targeting the mucosa.

Beyond easy access and the possibility for self-medication, the choice of buccal delivery as a tissue model in this work is motivated by better patient acceptability compared to other mucosal administration routes (*e.g.*, ocular, vaginal, rectal), lower enzymatic activity, a lower propensity of the therapeutic to be washed away by saliva compared to sublingual administration, and that the device, which can simply be mounted on the inner surface of the lip (Fig. 1a), can easily and quickly be removed in the event of an adverse allergic reaction.[70–72] Moreover, buccal delivery has received far less attention compared to other mucosal routes given that there are challenges that have yet to be overcome, such as the low permeability through the stratified squamous epithelial cells[73] despite the buccal and sublingual tissue being among the most permeable of the oral mucosal membranes.[74] Further, buccal dosing to date has primarily been limited to sprays, tablets and chewing gum in conjunction with the use of chemical permeation enhancers.[9] An effective physical permeabilisation method driven by external forcing has, to our best knowledge, yet to be proposed. Nonetheless, we note that the present method, which simply relies on contact of the acoustic device with the mucosal surface—conceptually illustrated by a portable, battery-powered handheld applicator in Fig. 1a, can easily be extended for delivery *via* the other mucosal routes.

2 Materials and methods

2.1 Chemicals

All chemicals were purchased from Sigma Aldrich Pty. Ltd. (Mulgrave, VIC, Australia) unless specified otherwise. Specifically, we procured fluorescein sodium salt (fluorescein), fluorescein isothiocyanate (FITC)-labelled albumin, FITC-labelled dextran (20, 40 and 70 kDa), Hoechst 33342 stain, Tris buffer base, hydrochloric acid (HCl), Krebs-Ringer bicarbonate buffer, sucrose, isopentane, horseradish peroxidase (HRP), hydrogen peroxide (H_2O_2), 3,3′,5,5′-tetramethylbenzidine (TMB), ultrapure water, cotton gauze, paraformaldehyde (PFA, 20% v/v; Electron Microscopy Sciences, Emgrid Pty. Ltd., Gulfview Heights, SA, Australia), optimum cutting temperature solution (OCT; Proscitech Ltd., Kirwan, QLD, Australia), formalin (Proscitech Ltd., Kirwan, QLD, Australia), xylene (Hurst Scientific, Forrestdale, WA, Australia), haematoxylin (Australian Biostain, Traralgon, VIC, Australia), Scott's tap

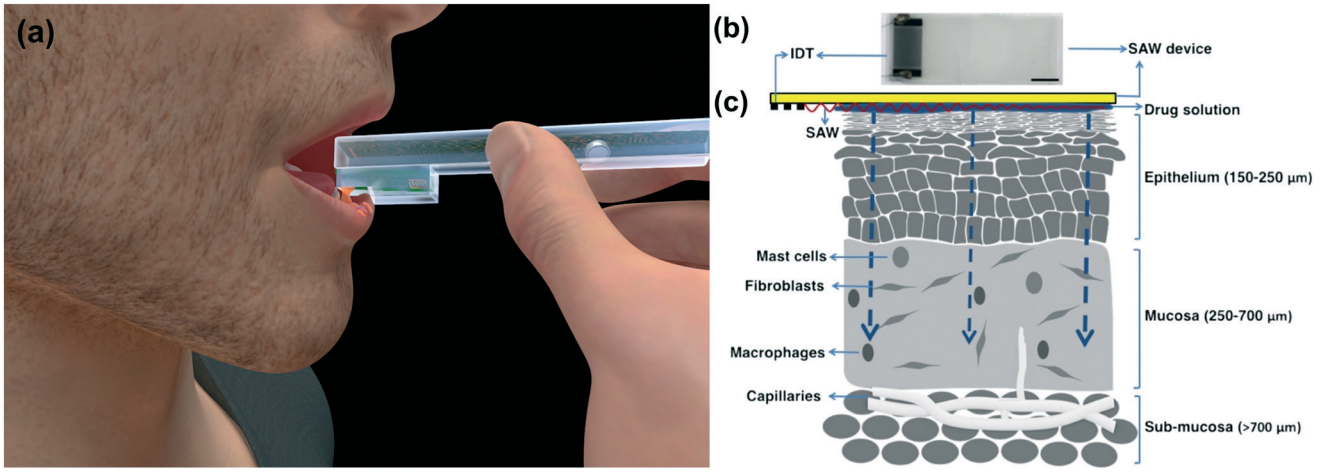

Fig. 1 (a) Idealised depiction illustrating the proposed concept of a portable handheld applicator device for mucosal delivery; the image shows delivery *via* buccal administration although it can be envisaged that the concept can easily be adapted for other mucosal administration routes. (b) Top view image of the SAW device, and, (c) side view schematic of the experimental set up employed to demonstrate the delivery of therapeutic agents into different layers of a porcine lip tissue section. For optimum administration, the dose is ideally confined within the mucosal layer to a depth of 700 μm beneath the surface so as to minimise penetration into the vascular rich submucosal layer beyond this depth. The scale bar denotes a length of 10 mm.

water (Amber Scientific Pty. Ltd., Midvale, WA, Australia), 1% aqueous eosin (Australian Biostain, Traralgon, VIC, Australia) and MM 24 Mounting Media (Leica Biosystems Inc., Buffalo Grove, IL, USA) for the experiments and histological staining.

2.2 SAW device fabrication

The SAW devices (Fig. 1b) consist of 127.86° *Y–X* rotated lithium niobate ($LiNbO_3$) single crystal piezoelectric substrates (Roditi Ltd., London, UK) on which 40 alternating 33- and 66-nm thick chromium–aluminium straight interdigitated transducer (IDT) electrodes (Fig. 1b) are photolithographically patterned using standard wet etching techniques. The SAW frequency—we examined 17, 30 and 55 MHz devices to explore their effect on the delivery whilst limiting the depth of perfusion to which the therapeutic molecules penetrate into the submucosa so that they are localised within the mucosal layer—is determined by setting the gap and width of the electrodes equal to $\lambda/4$, wherein λ = 234, 132 and 72 μm are the SAW wavelengths corresponding to these respective resonant frequencies. The fabricated devices were tested on a vector network analyser (VNA; ZVA, Rhode & Schwarz Pty. Ltd., North Ryde, NSW, Australia) prior to the start of the experiments. The application of an alternating electrical signal at resonance to the IDTs at various powers using a signal generator (SML01, Rhode & Schwarz Pty. Ltd., North Ryde, NSW, Australia) and amplifier (10W1000C, Amplifier Research, Souderton, PA, USA) then gives rise to a SAW, which propagates along the surface of the device.

2.3 Tissue model

Porcine lips (Fig. 1b) were acquired from a local abattoir and transported to the laboratory wrapped in gauze saturated with Krebs-Ringer bicarbonate buffer and maintained on ice at 4 °C to keep it viable and moist during transit. The lip tissues were subsequently separated from the underlying fat tissue to a thickness of approximately 0.3 cm by manual dissection with a sharp scalpel to minimise tissue damage. This was followed by washing with 1 M Tris-HCl buffer to ensure removal of debris and remnant blood on the surface. Cubes of approximately 0.5 cm × 0.5 cm × 0.3 cm were cut out from the entire lip and placed on a Petri dish containing gauze saturated with buffer until the end of the experiments. The experiments were performed within 2 hours from the time when the animals were sacrificed in the abattoir.

2.4 Model drug molecule perfusion

A 4 μl drop containing the model drug solution (120 ng of either fluorescein, FITC-dextran in MilliQ water or FITC-albumin in 10 mM Tris-HCl) was placed on the device prior to the start of the experiments. The device containing the drug solution atop it was then inverted and placed on a cube comprising the porcine lip sample with the epidermis facing the device, as schematically shown in Fig. 1c, following which the SAW at a specific frequency and power is excited over a given duration. The samples were washed immediately after exposure to the SAW, and the washed precipitate was collected to measure the drug loss. The clean tissue sample was then pat dried and immediately flash frozen in cryomolds pre-filled with OCT in the presence of liquid nitrogen cooled isopentane. The frozen samples were wrapped immediately with aluminium foil and stored at −80 °C, after which 50 μm thick layers of the samples were sectioned with a cryostat (HYRAX C60, Carl Zeiss AG, Oberkochen, Germany; CM1860, Leica Biosystems Inc.,

Buffalo Grove, IL, USA) parallel to the skin's surface at −18 °C. The tissue samples were protected from light at all times prior to the fluorescence measurements.

2.5 Histological staining

The frozen sections were cryotomed into 50 μm sections and air dried overnight at room temperature. The slides containing the sections were subsequently placed in 10% buffered formalin for 2 min under a fume hood. The slides were further washed with tap water followed by the addition of haematoxylin for 30 s. The haematoxylin was then removed with tap water, after which the slides were left in Scott's tap water for 30 s. A final staining step with 1% eosin for 30 s was conducted before carrying out a series of dehydration steps in ethanol followed by clearance with xylene. The dehydrated sections were finally mounted with MM 24 mounting media prior to analysis. Slides comprising tissue sections with perfused FITC-albumin were also counterstained with Hoechst 33342 (2 μg ml^{-1}) to specifically stain the cell nuclei, from which any condensation of the nuclear components could be observed.

2.6 Delivered dose

The sectioned layers were analysed under a microscope to capture fluorescent images at excitation wavelengths of 450–490 nm. All images were acquired under 10× magnification and 60 s of exposure. The mean fluorescence intensity of the images was calculated from the intensity of the green channel for each pixel using Image J® (National Institutes of Health, Bethesda, MD, USA). To account for any autofluorescence of the tissue, post-sectioned samples both in the absence and presence of the SAW, but without the addition of any fluorophore, were imaged to obtain the green channel pixel intensity. Given that the autofluorescence of both did not vary significantly, the unexposed samples were thus chosen as the control. The mean fluorescence intensity of this control sample for each 50 μm section was then subtracted from the samples exposed to the fluorescently-labelled model drug molecules under the SAW excitation. From a calibration standard, we were able to subsequently convert the mean fluorescence intensity into the mass of drug delivered to each section, which is normalised against the total amount of drug delivered to the entire sample, calculated from the total amount of drug deposited and accounting for any losses in the drug (*e.g.*, the residual drug on the device).

2.7 Temperature

Increases in temperature of the drug solution due to the SAW irradiation can lead to adverse effects on the structure and functionality of the therapeutic molecules to be delivered. We thus measured the temperature at the surface of the device using a temperature probe (HH506RA, OMEGA Engineering Inc., Norwalk, CT, USA) placed in contact with the surface of the device when the SAW is excited under the different parameters employed. We note that the solution temperature will be lower than that measured at the surface of the device and the temperature in the tissue lower than that in the solution.

2.8 Circular dichroism spectroscopy

The effect of the acoustic irradiation on the secondary α-helix structure of albumin (1 mg ml^{-1} BSA in 10 mM Tris-HCl buffer) was analysed by recording the difference in their absorption properties under polarised ultraviolet light following exposure to the SAW at different powers and durations corresponding to those used in the tissue delivery experiments. To avoid any denaturation by the salts in the buffer, we examined the circular dichroism (CD) spectra immediately after collection of the samples. The temperature was maintained at 20 °C throughout the experiment. A glass cuvette with a path length of 0.1 cm was chosen, and a 400 μl sample was exposed to UV in the wavelength range between 190 nm and 250 nm. In its unfolded state, the ellipticity of α-helical peptides in the protein is nearly zero over the wavelengths 209–222 nm corresponding to their absorption bond. On the other hand, the protein in its native state possesses a positive band at 193 nm and negative bands at 208 nm and 222 nm. Any shift in the band to an increasingly positive value between 209 and 222 nm therefore reveals the extent to which the α-helical structure is unfolded and hence the extent of conformational change in the protein.

2.9 Enzyme activity study

In addition to examining the post-irradiated BSA secondary structure, an enzyme activity study was also carried out to monitor the functional activity of enzymes exposed to the SAW. Briefly, HRP as a model enzyme was exposed to the SAW at the different powers and exposure times used in the tissue delivery experiments and collected in 10 mM sodium acetate buffer. The solution was then mixed with H_2O_2 and TMB. HRP then converts the colourless TMB substrate into a blue-coloured solution in the presence of H_2O_2. The absorbance at 652 nm, measured using a plate reader (Spectramax® Paradigm multimode plate reader, Molecular Devices LLC, Sunnyvale, CA, USA), is directly proportional to the activity of the enzyme, which, in turn, provides an indication of its functional integrity following excitation with the SAW.

3 Results and discussion

Fig. 2 shows a representative result, in which fluorescently-labelled FITC-albumin is infused into the porcine buccal tissue under the SAW excitation compared to that for the case of passive diffusion. It can be seen that not only considerably more protein is delivered into the tissue when it is exposed to the SAW irradiation than if it were left to solely diffuse into the tissue over the same duration, but that the protein delivered also penetrates significantly deeper into the tissue. The poor delivery due to passive diffusion can primarily be

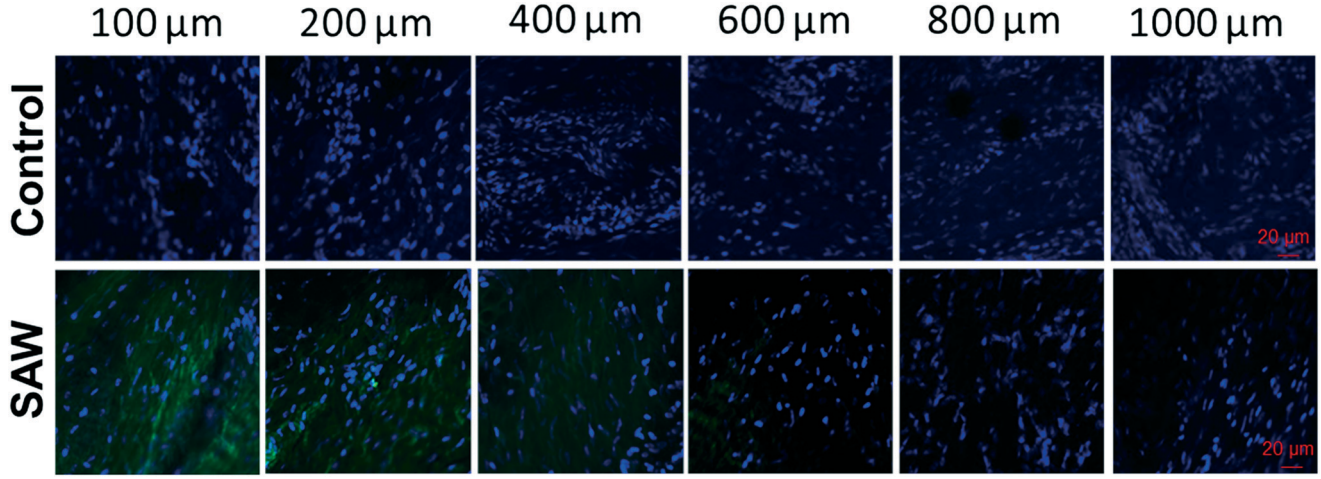

Fig. 2 Distribution of FITC-albumin (green) in selected tissue sections at various depths from the surface of the porcine lip. The top row images comprise the result from the control experiments when the protein is allowed to diffuse into the tissue over a duration of 10 s. The bottom row images comprise the result when the SAW at a frequency of 30 MHz and an input voltage of 50 mV is employed to infuse the protein into the tissue for 10 s. The cell nuclei are counterstained by Hoechst 33342 (blue).

attributed to the existence of the stratified squamous epithelium, which makes up the bulk of the lip tissue lining beneath the very thin stratum corneum. Given that it predominantly consists of epithelial cells[72] whose lateral interstitial spaces comprising tight junctions between the cells only allow the through passage of small hydrophilic molecules, it is unlikely that large hydrophilic protein molecules such as FITC-albumin navigate this tortuous paracellular pathway.[75,76] Moreover, even if the intercellular spaces are sufficiently large to facilitate entry of the protein molecules, the diffusion time scale, which is on the order of hours, is considerably longer than the duration over which the images in Fig. 2 were acquired. Consequently, it is unsurprising that negligible drug is present in the tissue in the control sample, at least over these short times.

On the contrary, we observe rapid penetration of the drug into the tissue when it is exposed to the SAW irradiation, wherein the protein molecules are phoretically driven through the intercellular spaces due to the acoustic radiation pressure imparted on them. This radiation pressure arises as a consequence of the sound waves that are generated in the drug solution when the SAW energy leaks into it from the surface of the device.[22,77] The delivery into the tissue is possibly further aided by permeabilisation of the mucosal membrane due to the vibration directly induced on it by the SAW irradiation.[69,78] This then results in increased intercellular spacing due to structural reorganisation of the lipids in the intercellular domains to an extent that it sufficiently permits the passage of larger molecules which would otherwise not have perfused through.[69,79–82]

It should be noted though that such lipid structure reorganisation is not accompanied by pore formation—this is because cavitation, which is the predominant mechanism by which membrane pores are generated under sonoporation at low kHz order frequencies, is absent at the high MHz order frequencies employed.[69,83,84] The lack of pore formation here is an advantage as a high level of cell and tissue viability is retained below a threshold input voltage of 100 mV (Fig. 3), thus minimising tissue scarring following exposure to the SAW. This is confirmed by the absence of nuclear condensation, which is proportional to the extent of cell apoptosis in the tissue, as seen from the nuclear staining in the images; such condensation, resulting in bright clumps of the nuclei,[85,86] on the other hand, was evident at 100 mV. In any case, increasing the input voltage to this threshold level does not lead to significant benefit in terms of the delivered dose. Alternatively, or possibly in combination with such enhanced paracellular transport under SAW excitation, it is conceivable that the acoustic radiation pressure enables the protein molecules to be transported through the cells *via* the transcellular pathway,[87–89] particularly given that SAW irradiation of cells has been recently shown to reversibly and instantaneously enhance the permeability of cell membranes, thus facilitating fast transport into, and, subsequently, out of, cells.[69]

As expected, the delivered dose can be seen in Fig. 4a and e and 5a and e to decay with increasing depth into the tissue, as observed from the decrease in the fluorescence intensity in successive tissue sections (Fig. 2). We now turn our attention to optimising the device parameters associated with the delivery such that the decay in the dose occurs over a length associated with the thickness of the mucosal layer in order that the delivery to this region is maximised whilst minimising the amount of drug delivered to further depths into the submucosa. Fig. 4 and 5, for example, show the respective concentration profiles of fluorescein and FITC-albumin in the sectioned tissues for different SAW powers and exposure durations, in which we observe that the delivered dose is mainly confined to a depth of approximately 850 μm from the lip surface for fluorescein (Fig. 4d), and around 750 μm for FITC-albumin (Fig. 5d), thus confirming the ability of the method for localising most of the

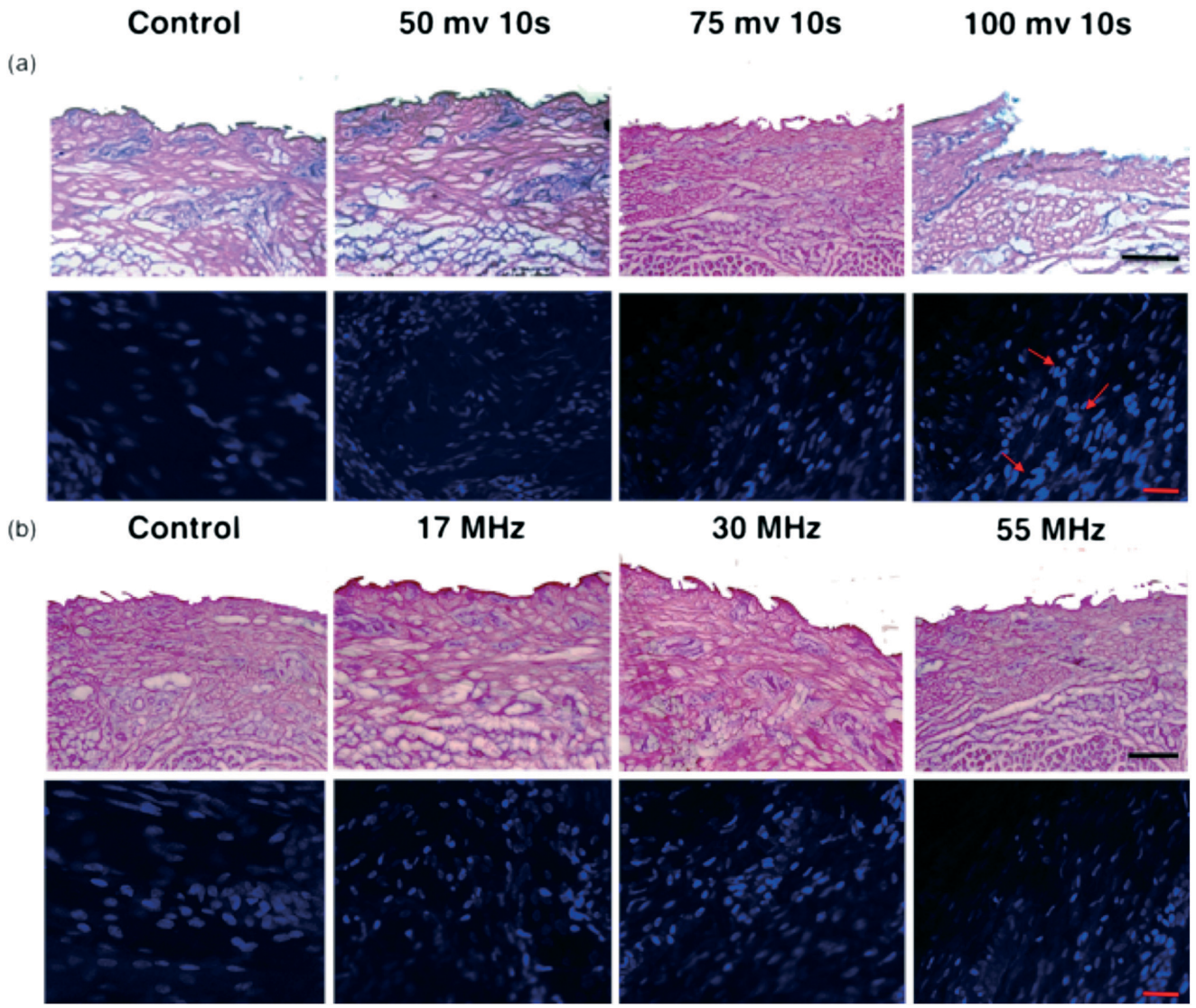

Fig. 3 (Top rows) Hematoxylin & eosin (H&E) staining of the porcine buccal tissue showing the morphological structure of the mucosal layer before (control) and after exposure to SAW irradiation at (a) different input voltages, and, (b) SAW frequencies, over a duration of 10 s. In (a), the SAW frequency is held constant at 30 MHz, whereas in (b), the input voltage is fixed at 50 mV. The stratified squamous epithelial layer, comprising the topmost layer, can clearly be seen to be intact in the absence of SAW (control) and at power levels below 100 mV at which there is considerable disruption of the cells in this layer. This can be seen from the nuclear staining (blue; bottom rows) in which condensation of the cell nuclei is evident at 100 mV, as indicated by the arrows. The scale bar denotes a length of 275 μm for the H&E stained images and 20 μm for the nuclei stained images, respectively.

delivered therapeutic to the mucosa, which, in the case of porcine lips, is approximately 700 μm thick.[90] This ability to rapidly, but yet controllably, enhance the delivery of therapeutic agents—in particular, large molecules which do not normally penetrate the epithelial barrier of the stratum corneum or the squamous epithelium layer into tissue on their own *via* passive diffusion, as seen from the control experiments, and, at the same time, avoiding driving them too deep into the submucosal layer, then represents a significant advance over other techniques, especially those for transdermal delivery, which primarily have been designed to achieve the greatest penetration possible.

Fig. 4b and f show that although it is possible to achieve a fourfold increase in the dose of fluorescein and at greater penetration depths while still maintaining localisation primarily in the mucosal layer compared to that achieved by pure diffusion in the absence of the acoustic irradiation (control), there is little effect of the SAW power and exposure duration in the amount of fluorescein delivered or the depth to which it penetrates in the tissue. In addition, we observe around 99% efficiency in the delivery (Fig. 4c and g), *i.e.*, almost all of the 120 ng of fluorescein in the feedstock solution is delivered into the tissue; the majority of this (≈94.2%) being confined within the mucosa, which comprises the first 700 μm section immediately beneath the surface of the lip (Fig. 4b and f). This is likely because fluorescein is a small molecule (M_w = 376 g mol^{-1}) that is easily transported either *via* the paracellular or transcellular routes once the acoustic irradiation initially facilitates their passage through the

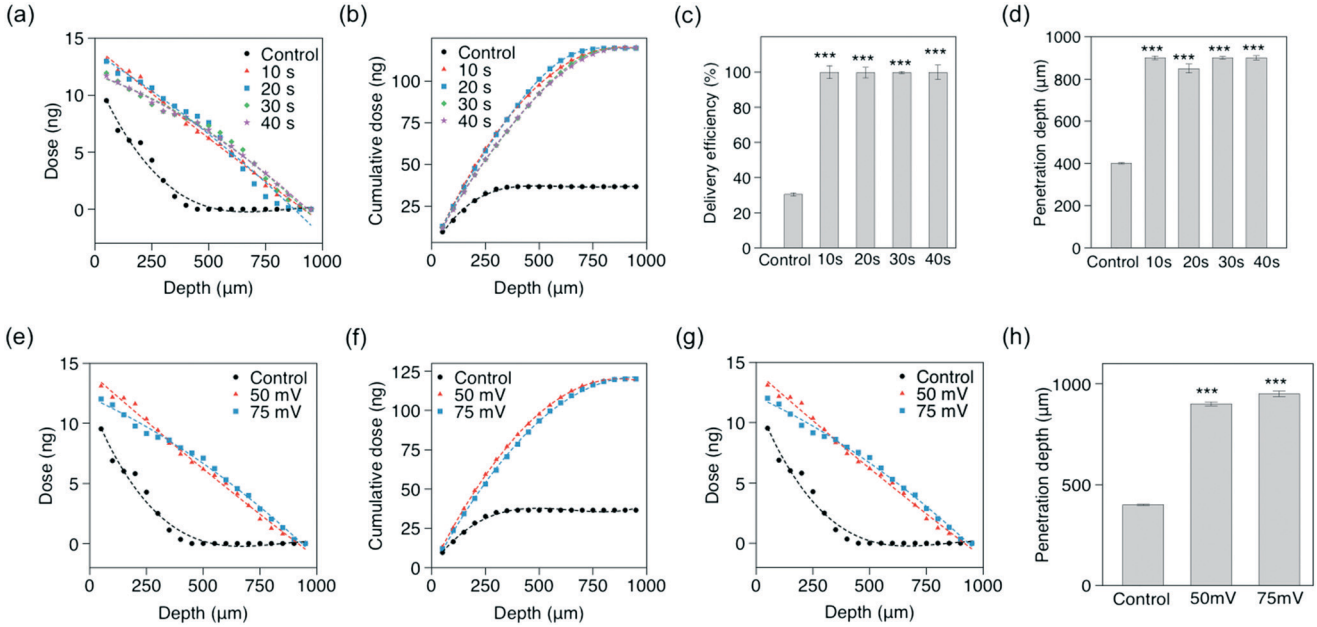

Fig. 4 Effect of the SAW (a–d) exposure duration, and, (e–h) input voltage, on the delivery of fluorescein to porcine lip tissue. The same data is represented in terms of (a and e) dose, and, (b and f) cumulative dose distributions, (c and g) delivery efficiencies, and, (d and h) penetration depths. The SAW frequency and the initial amount of fluorescein in the feedstock solution is fixed at 30 MHz and 120 ng, respectively. In (a–d), the input voltage is fixed at 50 mV, whereas in (e–h), the exposure duration is fixed at 10 s. The control experiment involves exposing the tissue to fluorescein using the same setup and over the same exposure duration, but in the absence of the SAW forcing. The data are represented in terms of a mean value (n = 3) ± the standard error. The asterisks *** indicate statistically significant differences compared to the control with $p < 0.001$.

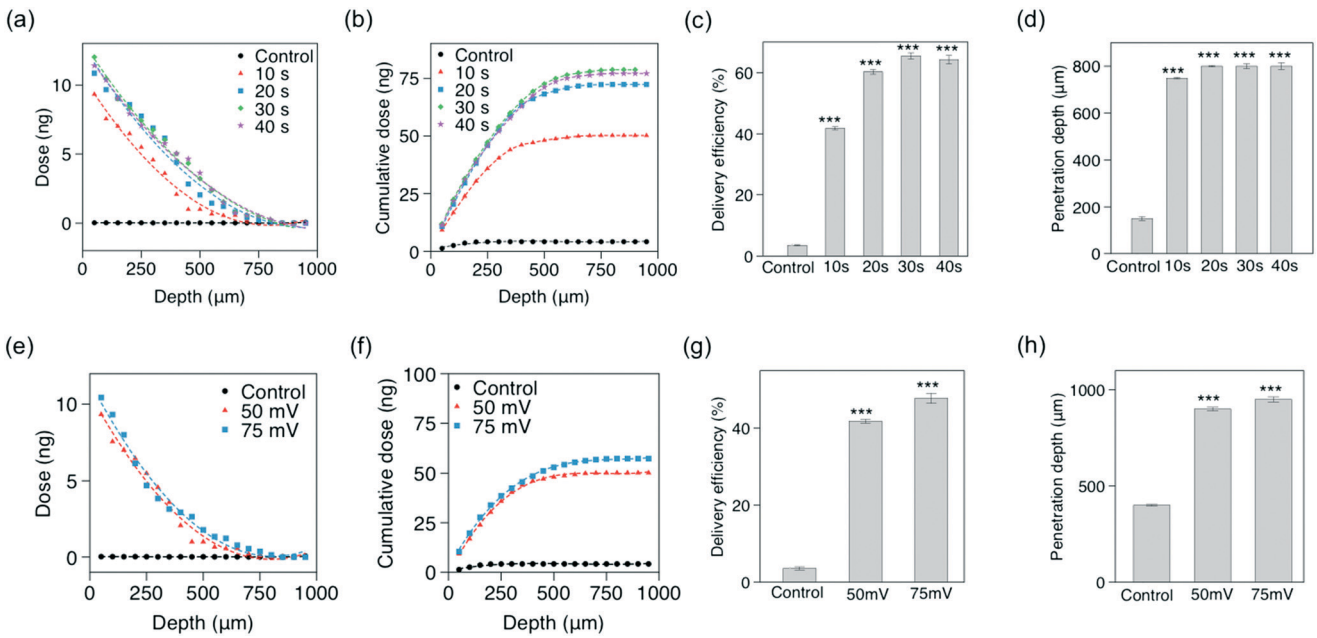

Fig. 5 Effect of the SAW (a–d) exposure duration, and, (e–h) input voltage, on the delivery of FITC-albumin to porcine lip tissue. The same data is represented in terms of (a and e) dose, and, (b and f) cumulative dose distributions, (c and g) delivery efficiencies, and, (d and h) penetration depths. The SAW frequency and the initial amount of FITC-albumin in the feedstock solution is fixed at 30 MHz and 120 ng, respectively. In (a–d), the input voltage is fixed at 50 mV, whereas in (e–h), the exposure duration is fixed at 10 s. The control experiment involves exposing the tissue to FITC-albumin using the same setup and over the same exposure duration, but in the absence of the SAW forcing. The data are represented in terms of a mean value (n = 3) ± the standard error. The asterisks *** indicate statistically significant differences compared to the control with $p <$ 0.001.

intercellular spaces in the epithelium that makes up a large part of the mucosal layer.

The effect of the SAW power and exposure duration, on the other hand, is more pronounced for FITC-albumin

(Fig. 5), particularly given that it is a considerably larger (66 kDa) and more complex molecule. In particular, we observe a marked difference between 10 and 20 s of exposure time in which approximately 50% increase in the dose was observed simply by increasing the exposure time (Fig. 5b). The overall delivery efficiency—essentially up to around 60% (Fig. 5c and g)—is lower compared to that for fluorescein (Fig. 4c and g), which is expected given the large molecular size of the protein, although we note that most of the drug is effectively distributed within the mucosal layer; neither the SAW power or exposure duration appeared to have much effect on the penetration depth to which the drug is delivered. We note that even though some drug penetrates beyond 700 μm (Fig. 5d and h)—the approximate thickness of the buccal mucosa in pigs—into the submucosal layer, this is minimal since it can be seen from the cumulative distribution in Fig. 5b and f that the majority of the drug is delivered to a depth of approximately 500 μm from the surface, as observed from the rapid plateauing of the distribution beyond this depth.

The role of the SAW frequency can be seen in Fig. 6. All other parameters being equal, we observe the penetration depth to decrease from approximately 1 mm to 700 μm and 550 μm when the SAW frequency is increased from 17 MHz to 30 and 55 MHz, respectively (Fig. 6d). This is because the viscous attenuation length of the sound wave transmitted into the tissue scales inversely with frequency, and hence the sound wave is able to travel further into the tissue before it

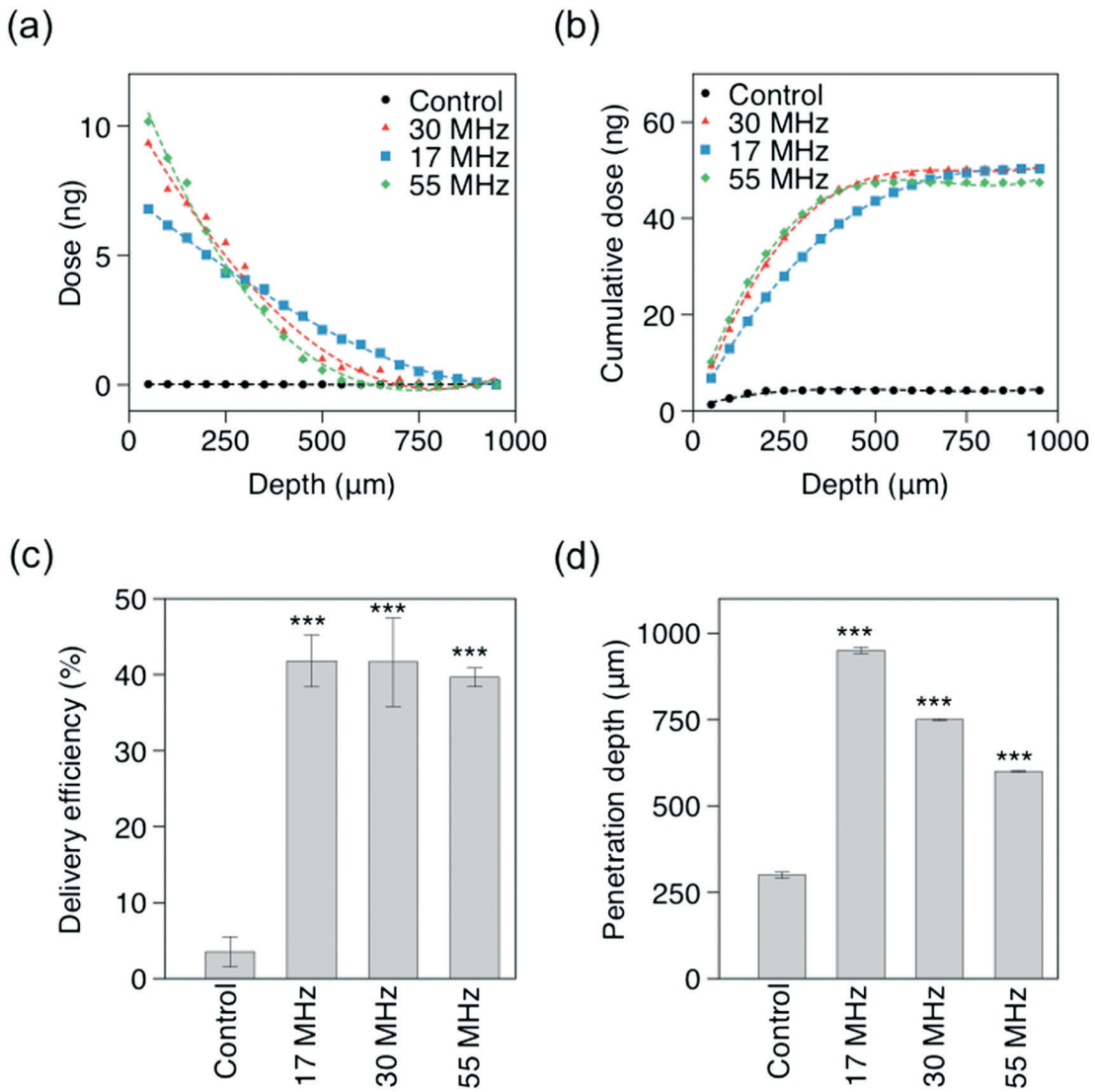

Fig. 6 Effect of the SAW frequency on the delivery of FITC-albumin to porcine lip tissue. The same data is represented in terms of (a) dose, and, (b) cumulative dose distributions, (c) delivery efficiencies, and, (d) penetration depths. The initial amount of FITC-albumin in the feedstock solution, as well as the SAW input voltage and exposure duration are fixed at 120 ng, 50 mV and 10 s, respectively. The control experiments involved exposing the tissue to FITC-albumin using the same setup and over the same exposure duration, but in the absence of the SAW forcing. The data are represented in terms of a mean value (n = 3) ± the standard error. The asterisks *** indicate statistically significant differences compared to the control with $p < 0.001$.

decays. The effect is however less pronounced for the amount of drug delivered and hence the efficiency of the delivery although we note that the distribution of the drug delivered to the tissue is more uniform with lower frequencies. Practically, there exists a trade-off between the penetration depth and the amount delivered, as well as the distribution of the drug in the tissue when choosing the operating frequency. For example, while all of the drug can be localised in the buccal mucosal layer up to a thickness of 700 μm with either the 30 or 55 MHz devices, the 30 MHz device provides a slightly longer penetration depth such that some of the drug is deposited in the region between a depth of 550 to 700 μm (Fig. 6b). Further, it can be seen from Fig. 6b that the amount of drug delivered and hence the efficiency of delivery to the mucosal layer up to a thickness of 700 μm is more or less similar across all three frequencies. As such, if deposition of the drug in the submucosal layer beyond 700 μm is not critical, it may be preferable to adopt the lower 17 MHz frequency in order to achieve a more uniform distribution throughout the mucosal layer.

To further elucidate the effect of the size of the therapeutic agent on the efficacy of delivery, we repeated the experiments with FITC-labelled dextrans—simple hydrophilic glucopolysaccharide molecules—with varying molecular weights (20, 40 and 70 kDa) for 30 MHz SAW at 50 mV over 10 s (Fig. 7). As seen in Fig. 7a, only minimal molecular penetration was observed in the control experiments that were conducted in the absence of the SAW excitation regardless of the size of the molecule: only 3.59 ng, equivalent to an efficiency of 2.99%, was delivered to the tissue over a depth of approximately 300 μm in 10 s (Fig. 7b–d), underscoring not only the slow diffusion process but also the inability for the molecules to penetrate into the tissue beyond a superficial depth without the aid of external forcing. In contrast, and

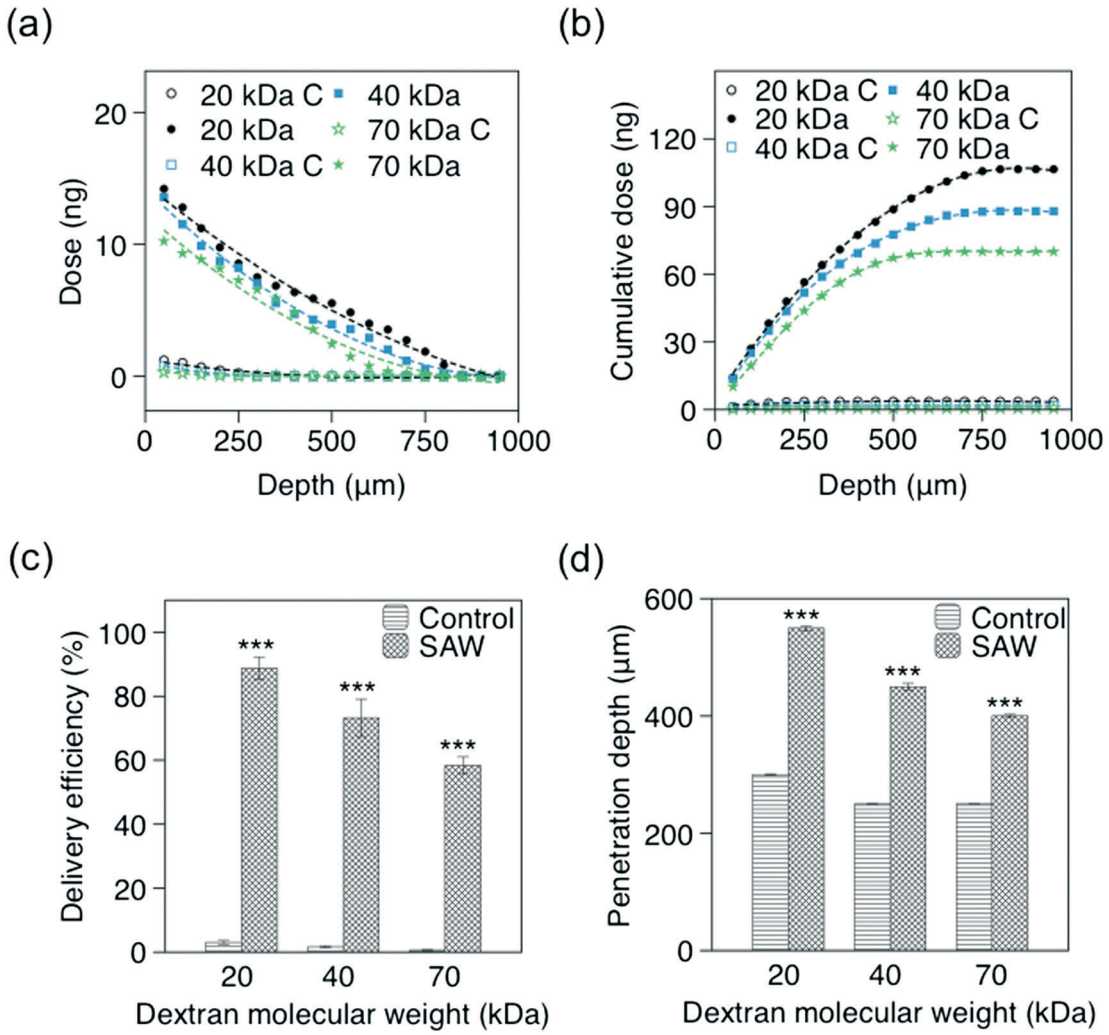

Fig. 7 Delivery of FITC-dextrans of different molecular weights (20, 40 and 70 kDa) to porcine lip tissue. The same data is represented in terms of (a) dose, and, (b) cumulative dose distributions, (c) delivery efficiencies, and, (d) penetration depths. The initial amount of FITC-dextran in the feedstock solution, as well as the SAW frequency, input voltage and exposure duration are fixed at 120 ng, 30 MHz, 50 mV and 10 s, respectively. The control experiments (labelled 'C' in the legends) involve exposing the tissue to the different FITC-dextrans using the same setup and over the same exposure duration, but in the absence of the SAW forcing. The data are represented in terms of a mean value (n = 3) ± the standard error. The asterisks *** indicate statistically significant differences compared to the control with $p < 0.001$.

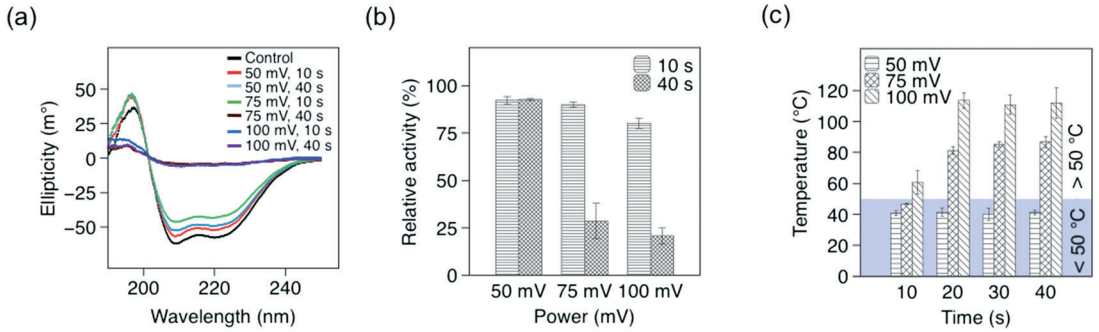

Fig. 8 (a) Circular dichroism (CD) spectra showing the α-helix structure of albumin after their exposure to different levels and durations of the SAW irradiation. (b) Activity of HRP exposed to the SAW irradiation at different levels and over different times, normalised against that of the unexposed control. (c) Corresponding temperatures to which the SAW device is heated (this value being the maximum in the temperature rise; in other words, the solution temperature will always be lower than that at the surface of the device and the temperature in the tissue lower than that in the solution) for different input voltages and exposure times.

consistent with the abovementioned fluorescein and FITC-albumin results in the presence of the SAW, the delivery to the tissue is significantly enhanced both in terms of the penetration depth and the amount that is delivered (*i.e.*, the

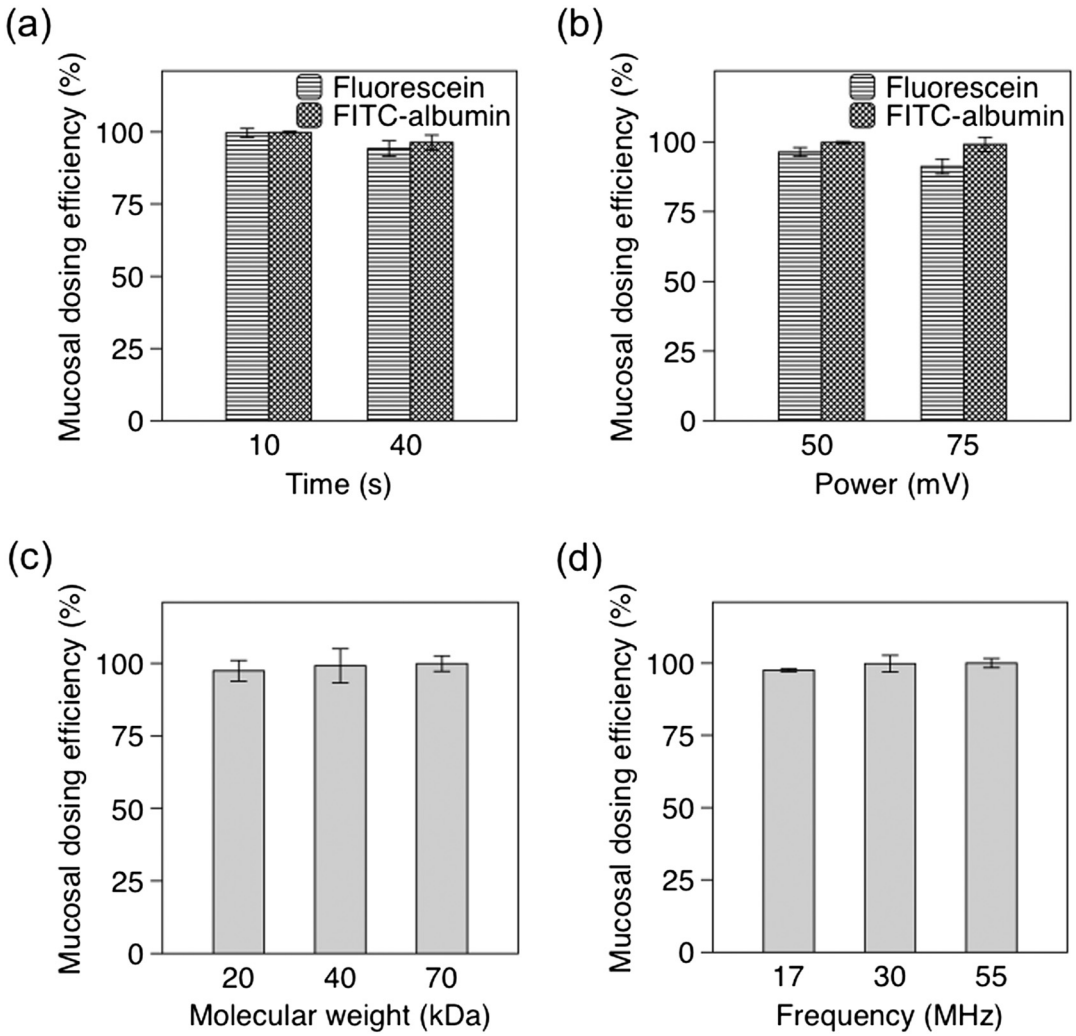

Fig. 9 Efficiency of delivering fluorescein, FITC-albumin and FITC-dextran *solely* to the mucosa (assumed to comprise the topmost 700 μm-thick layer from the surface[90]) of buccal porcine tissue, as a function of various system parameters: (a) SAW exposure duration, (b) input voltage to the SAW device, (c) FITC-dextran molecular weight, and, (d) SAW frequency. Unless varied as part of the study, the SAW frequency, input voltage and exposure duration are maintained at 30 MHz, 50 mV and 10 s, respectively.

delivery efficiency). We note that the amount of dextran delivered to the tissue decreases linearly from approximately 110 ng to 70 ng when the molecular size is increased from 20 to 70 kDa, corresponding to a decrease in the delivery efficiency from around 90% to 60% (Fig. 7b and c). Additionally, the penetration depth also decreases approximately linearly from around 600 μm to around 400 μm (Fig. 7d). Parenthetically, it is interesting to note that under the same SAW excitation parameters, the penetration depth and delivery efficiency for 70 kDA FITC-dextran are close to that for FITC-albumin, which is similar in molecular weight despite it being far more complex than the simple branched structure of dextran molecules, therefore suggesting the dominance of the role of the size rather than the structure of the molecule in the delivery.

Finally, we verify that the applied acoustic irradiation does not lead to adverse effects on the structure of the protein during delivery into the tissue, particularly given that the absorption of the sound waves in the feedstock solution, and to a lesser extent in the tissue, leads to some heating, which could potentially denature the protein. This was carried out by accessing the secondary structure of albumin that has been exposed to different levels and exposure durations of the SAW irradiation *via* CD spectroscopy. As can be seen in Fig. 8a, increasing levels of protein denaturation in terms of the unfolding of their α-helix structure can be observed as the temperature of the feedstock solution increases with either prolonged exposure or increasing intensity of the SAW irradiation. We note that this is minimal (<10%) at 50 mV across all the exposure durations examined in this work. At the higher input of 75 mV, the structural damage to the protein is still minimal (<15%) if the exposure duration is limited to 10 s. This is encouraging given that these are the input parameters to the SAW that are primarily required in order to obtain sufficiently high doses of the protein into the tissue, whilst maximising their localisation within the mucosal layer (Fig. 5) and minimising damage to the tissue structure (Fig. 3). Consistent with the earlier results in Fig. 3, further increases of the irradiation beyond the threshold limit, however, led to significant disordering of the protein conformation. These results were reflected in the examination of post-exposure enzymatic activity in Fig. 8b, which showed that significant decreases in activity only occurred with sufficiently high temperature rises beyond 50 °C (Fig. 8c) when the HRP was exposed to the SAW irradiation over prolonged periods.

4 Conclusion

With the steady rise in the advent of various infectious diseases and antibiotic immune pathogens, the need for better protective immunisation is necessary to improve the quality of human life. While a number of delivery methods have been demonstrated for immunisation *via* delivery through tissue, it is still a significant challenge to localise the therapeutic agent within the mucosa where it can be taken up by the abundance of innate and adaptive immune system cells in the mucosa-associated lymphoid tissue to elicit a local mucosal immune response, rather than being delivered deeper into the vascularised submucosal layers where it is taken up by the circulation, which then results in a weaker systemic immune response. Ultrasonic methods at lower (<1 MHz) frequencies that rely on cavitation to effect cellular poration or generate significant pressures to force the therapeutic molecules into the tissue, for example, tend to result in excessive molecular penetration depths into the submucosa owing to the extremely large cavitation pressures and long sound attenuations lengths; sonoporation, whilst facilitating easier transcellular passage, however, also results in poor cellular viability and tissue scarring.

Motivated by the lack of physical methods to localise and hence maximise drug delivery to the mucosal layers of tissue, we have demonstrated a novel method to achieve this by employing high frequency (>10 MHz) SAWs, in which cavitation is absent and which possesses shorter acoustic attenuation lengths. In particular, we show that the method is able to deliver much higher doses of model therapeutic molecules —commensurate with the 50–500 ng of protein, for example, that is typically delivered to induce mucosal immunity in adult humans[91,92]—into porcine buccal tissue and at much higher rates compared to the control, which depended solely on passive diffusion—a rather slow process that is also often unable to facilitate the passage of large molecules such as proteins through the epithelium. More importantly, we show the ability to avoid delivering the therapeutic agent too far into the submucosa so as to localise their dose within the mucosa, which, for porcine buccal tissue, comprises the topmost layer beneath the surface to a depth of 700 μm.[90] This is summarised in Fig. 9 which shows the efficiency of dosing the drug solely in the mucosal layer. It can be seen that mucosal dosing efficiencies over 95% can be achieved for SAW irradiation levels and exposure durations that do not lead to protein denaturation.

Conflicts of interest

There are no conflicts to declare.

Acknowledgements

ARR is grateful for an RMIT University Vice-Chancellor's Postdoctoral Fellowship and LYY for an Australian Research Council (ARC) Future Fellowship (FT130100672). LYY also acknowledges funding from the ARC through Discovery Project (DP170101061).

References

1 M. R. Neutra, E. Pringault and J.-P. Kraehenbuhl, *Annu. Rev. Immunol.*, 1996, **14**, 275–300.
2 J. R. McGhee, J. Mestecky, M. T. Dertzbaugh, J. H. Eldridge, M. Hirasawa and H. Kiyono, *Vaccine*, 1992, **10**, 75–88.
3 J. M. Wells and A. Mercenier, *Nat. Rev. Microbiol.*, 2008, **6**, 349.

4 L. Wang, Y. Zhou, M. Wu, M. Wu, X. Li, X. Gong, J. Chang and X. Zhang, *Nanomedicine*, 2018, **13**, 69–88.
5 J. Holmgren and C. Czerkinsky, *Nat. Med.*, 2005, **11**, S45–S53.
6 N. Lycke, *Nat. Rev. Immunol.*, 2012, **12**, 592–605.
7 A. K. Shakya, M. Y. Chowdhury, W. Tao and H. S. Gill, *J. Controlled Release*, 2016, **240**, 394–413.
8 P. Brandtzaeg, *Immunol. Invest.*, 2010, **39**, 303–355.
9 H. Kraan, H. Vrieling, C. Czerkinsky, W. Jiskoot, G. Kersten and J.-P. Amorij, *J. Controlled Release*, 2014, **190**, 580–592.
10 K. A. Woodrow, K. M. Bennett and D. D. Lo, *Annu. Rev. Biomed. Eng.*, 2012, **14**, 17–46.
11 Y. Fukuyama, D. Tokuhara, K. Kataoka, R. S. Gilbert, J. R. McGhee, Y. Yuki, H. Kiyono and K. Fujihashi, *Expert Rev. Vaccines*, 2012, **11**, 367–379.
12 S. K. Lai, Y.-Y. Wang and J. Hanes, *Adv. Drug Delivery Rev.*, 2009, **61**, 158–171.
13 S. Ferrari, C. Kitson, R. Farley, R. Steel, C. Marriott, D. A. Parkins, M. Scarpa, B. Wainwright, M. J. Evans, W. H. Colledge, D. M. Geddes and E. W. Alton, *Gene Ther.*, 2001, **8**, 1380–1386.
14 M. O. Henke and F. Ratjen, *Paediatr. Respir. Rev.*, 2007, **8**, 24–29.
15 C. M. Schoellhammer and G. Traverso, *Expert Opin. Drug Delivery*, 2016, **13**, 1045–1048.
16 C. M. Schoellhammer, G. Y. Lauwers, J. A. Goettel, M. A. Oberli, C. Cleveland, J. Y. Park, D. Minahan, Y. Chen, D. G. Anderson, A. Jaklenec and S. B. Snapper, *Gastroenterology*, 2017, **152**, 1151–1160.
17 R. Alvarez-Román, G. Merino, Y. Kalia, A. Naik and R. Guy, *J. Pharm. Sci.*, 2003, **92**, 1138–1146.
18 H. Ueda, M. Mutoh, T. Seki, D. Kobayashi and Y. Morimoto, *Biol. Pharm. Bull.*, 2009, **32**, 916–920.
19 M. R. Prausnitz and R. Langer, *Nat. Biotechnol.*, 2008, **26**, 1261–1268.
20 S. N. Andrews, E. Jeong and M. R. Prausnitz, *Pharm. Res.*, 2013, **30**, 1099–1109.
21 J. Friend and L. Y. Yeo, *Rev. Mod. Phys.*, 2011, **83**, 647–704.
22 L. Y. Yeo and J. R. Friend, *Annu. Rev. Fluid Mech.*, 2014, **46**, 379–406.
23 C. Huh, M. Bhutani, E. Farfan and W. Bolch, *Physiol. Meas.*, 2003, **24**, N15–22.
24 P. W. Morrison and V. V. Khutoryanskiy, *Mucoadhes. Mater. Drug Delivery Syst.*, 2014, 39–60.
25 A. Balica, D. Wald-Spielman, K. Schertz, S. Egan and G. Bachmann, *Maturitas*, 2017, **102**, 69–72.
26 X. Ding, P. Li, S.-C. S. Lin, Z. S. Stratton, N. Nama, F. Guo, D. Slotcavage, X. Mao, J. Shi, F. Costanzo and T. J. Huang, *Lab Chip*, 2013, **13**, 3626–3649.
27 G. Destgeer and H. J. Sung, *Lab Chip*, 2015, **15**, 2722–2738.
28 D. B. Go, M. Z. Atashbar, Z. Ramshani and H.-C. Chang, *Anal. Methods*, 2017, **9**, 4112–4134.
29 P. Li, Z. Mao, Z. Peng, L. Zhou, Y. Chen, P.-H. Huang, C. I. Truica, J. J. Drabick, W. S. El-Deiry, M. Dao and S. Suresh, *Proc. Natl. Acad. Sci. U. S. A.*, 2015, **112**, 4970–4975.
30 G. Destgeer, B. H. Ha, J. Park, J. H. Jung, A. Alazzam and H. J. Sung, *Anal. Chem.*, 2015, **87**, 4627–4632.
31 J. Behrens, S. Langelier, A. R. Rezk, G. Lindner, L. Y. Yeo and J. R. Friend, *Lab Chip*, 2015, **15**, 43–46.
32 D. J. Collins, C. Devendran, Z. Ma, J. W. Ng, A. Neild and Y. Ai, *Sci. Adv.*, 2016, **2**, e1600089.
33 M. Wu, Z. Mao, K. Chen, H. Bachman, Y. Chen, J. Rufo, L. Ren, P. Li, L. Wang and T. J. Huang, *Adv. Funct. Mater.*, 2017, **27**, 1606039.
34 A. Wixforth, C. Strobl, C. Gauer, A. Toegl, J. Scriba and Z. v. Guttenberg, *Anal. Bioanal. Chem.*, 2004, **379**, 982–991.
35 A. Renaudin, P. Tabourier, V. Zhang, J. Camart and C. Druon, *Sens. Actuators, B*, 2006, **113**, 389–397.
36 T. Franke, A. R. Abate, D. A. Weitz and A. Wixforth, *Lab Chip*, 2009, **9**, 2625–2627.
37 M. Baudoin, P. Brunet, O. Bou Matar and E. Herth, *Appl. Phys. Lett.*, 2012, **100**, 154102–154102.
38 S. Collignon, J. Friend and L. Yeo, *Lab Chip*, 2015, **15**, 1942–1951.
39 A. Bussonnière, M. Baudoin, P. Brunet and O. B. Matar, *Phys. Rev. E*, 2016, **93**, 053106.
40 M. Sesen, C. Devendran, S. Malikides, T. Alan and A. Neild, *Lab Chip*, 2017, **17**, 438–447.
41 J. Park, J. H. Jung, K. Park, G. Destgeer, H. Ahmed, R. Ahmad and H. J. Sung, *Lab Chip*, 2018, **18**, 422–432.
42 Z. v. Guttenberg, A. Rathgeber, S. Keller, J. Rädler, A. Wixforth, M. Kostur, M. Schindler and P. Talkner, *Phys. Rev. E: Stat., Nonlinear, Soft Matter Phys.*, 2004, **70**, 056311.
43 S. Girardo, M. Cecchini, F. Beltram, R. Cingolani and D. Pisignano, *Lab Chip*, 2008, **8**, 1557–1563.
44 M. Tan, L. Yeo and J. Friend, *EPL*, 2009, **87**, 47003.
45 L. Masini, M. Cecchini, S. Girardo, R. Cingolani, D. Pisignano and F. Beltram, *Lab Chip*, 2010, **10**, 1997–2000.
46 L. Schmid, A. Wixforth, D. A. Weitz and T. Franke, *Microfluid. Nanofluid.*, 2012, **12**, 229–235.
47 S. M. Langelier, L. Y. Yeo and J. Friend, *Lab Chip*, 2012, **12**, 2970–2976.
48 L. Johansson, J. Enlund, S. Johansson, I. Katardjiev and V. Yantchev, *Biomed. Microdevices*, 2012, **14**, 279–289.
49 M. Miansari and J. R. Friend, *Adv. Funct. Mater.*, 2016, **26**, 7861–7872.
50 L. M. Lee, X. Cui and C. Yang, *Biomed. Microdevices*, 2009, **11**, 951–958.
51 R. Shilton, M. K. Tan, L. Y. Yeo and J. R. Friend, *J. Appl. Phys.*, 2008, **104**, 014910.
52 N. R. Glass, R. J. Shilton, P. P. Chan, J. R. Friend and L. Y. Yeo, *Small*, 2012, **8**, 1881–1888.
53 A. M. Gracioso Martins, N. R. Glass, S. Harrison, A. R. Rezk, N. A. Porter, P. D. Carpenter, J. Du Plessis, J. R. Friend and L. Y. Yeo, *Anal. Chem.*, 2014, **86**, 10812–10819.
54 L. Alhasan, A. Qi, A. Al-Abboodi, A. Rezk, P. P. Chan, C. Iliescu and L. Y. Yeo, *ACS Biomater. Sci. Eng.*, 2016, **2**, 1013–1022.
55 D. J. Collins, Z. Ma, J. Han and Y. Ai, *Lab Chip*, 2017, **17**, 91–103.
56 G. Destgeer, J. H. Jung, J. Park, H. Ahmed and H. J. Sung, *Anal. Chem.*, 2016, **89**, 736–744.
57 M. K. Tan, J. R. Friend and L. Y. Yeo, *Phys. Rev. Lett.*, 2009, **103**, 024501.

58 M. Kurosawa, T. Watanabe, A. Futami and T. Higuchi, *Sens. Actuators, A*, 1995, **50**, 69–74.
59 A. Qi, L. Y. Yeo and J. R. Friend, *Phys. Fluids*, 2008, **20**, 074103.
60 J. Ju, Y. Yamagata, H. Ohmori and T. Higuchi, *Sens. Actuators, A*, 2008, **147**, 570–575.
61 J. Ho, M. K. Tan, D. B. Go, L. Y. Yeo, J. R. Friend and H.-C. Chang, *Anal. Chem.*, 2011, **83**, 3260–3266.
62 S. R. Heron, R. Wilson, S. A. Shaffer, D. R. Goodlett and J. M. Cooper, *Anal. Chem.*, 2010, **82**, 3985–3989.
63 D. J. Collins, O. Manor, A. Winkler, H. Schmidt, J. R. Friend and L. Y. Yeo, *Phys. Rev. E: Stat., Nonlinear, Soft Matter Phys.*, 2012, **86**, 056312.
64 A. Winkler, S. Harazim, D. Collins, R. Brünig, H. Schmidt and S. Menzel, *Biomed. Microdevices*, 2017, **19**, 9.
65 A. Qi, J. R. Friend, L. Y. Yeo, D. A. Morton, M. P. McIntosh and L. Spiccia, *Lab Chip*, 2009, **9**, 2184–2193.
66 A. E. Rajapaksa, J. J. Ho, A. Qi, R. Bischof, T.-H. Nguyen, M. Tate, D. Piedrafita, M. P. McIntosh, L. Y. Yeo and E. Meeusen, *et al.*, *Respir. Res.*, 2014, **15**, 60.
67 C. Cortez-Jugo, A. Qi, A. Rajapaksa, J. R. Friend and L. Y. Yeo, *Biomicrofluidics*, 2015, **9**, 1–10.
68 L. Alhasan, A. Qi, A. R. Rezk, L. Y. Yeo and P. P. Chan, *Integr. Biol.*, 2016, **8**, 12–20.
69 S. Ramesan, A. R. Rezk, C. Dekiwadia, C. Cortez-Jugo and L. Y. Yeo, *Nanoscale*, 2018, **10**, 13165–13178.
70 J. O. Morales and D. J. Brayden, *Curr. Opin. Pharmacol.*, 2017, **36**, 22–28.
71 J. O. Morales, K. R. Fathe, A. Brunaugh, S. Ferrati, S. Li, M. Montenegro-Nicolini, Z. Mousavikhamene, J. T. McConville, M. R. Prausnitz and H. D. Smyth, *AAPS J.*, 2017, **19**, 652–668.
72 T. Caon, L. Jin, C. M. Simões, R. S. Norton and J. A. Nicolazzo, *Pharm. Res.*, 2015, **32**, 1–21.
73 M. J. Rathbone, I. Pather and S. Şenel, in *Oral Mucosal Drug Delivery and Therapy*, Springer, 2015, pp. 17–29.
74 D. Harris and J. R. Robinson, *J. Pharm. Sci.*, 1992, **81**, 1–10.
75 S. Law, P. Wertz, D. Swartzendruber and C. Squier, *Arch. Oral Biol.*, 1995, **40**, 1085–1091.
76 P. W. Wertz, D. C. Swartzendruber and C. A. Squier, *Adv. Drug Delivery Rev.*, 1993, **12**, 1–12.
77 L. Y. Yeo and J. R. Friend, *Biomicrofluidics*, 2009, **3**, 012002.
78 T. Reusch, F. J. R. Schülein, J. D. Nicolas, M. Osterhoff, A. Beerlink, H. J. Krenner, M. Müller, A. Wixforth and T. Salditt, *Phys. Rev. Lett.*, 2014, **113**, 118102.
79 H. L. Casal and H. H. Mantsch, *Biochim. Biophys. Acta, Rev. Biomembr.*, 1984, **779**, 381–401.
80 B. Szalontai, Y. Nishiyama, Z. Gombos and N. Murata, *Biochim. Biophys. Acta, Biomembr.*, 2000, **1509**, 409–419.
81 M. Inaba, S. Franceschelli, I. Suzuki, B. Szalontai, Y. Kanesaki, D. A. Los, B. Maresca, H. Hayashi and N. Murata, *J. Biol. Chem.*, 2002, **278**, 12191–12198.
82 D. A. Los and N. Murata, *Biochim. Biophys. Acta, Biomembr.*, 2004, **1666**, 142–157.
83 Y. Zhou, K. Yang, J. Cui, J. Ye and C. Deng, *J. Controlled Release*, 2012, **157**, 103–111.
84 Z. Shen, A. Brayman, L. Chen and C. Miao, *Gene Ther.*, 2008, **15**, 1147–1155.
85 B. S. Cummings, L. P. Wills and R. G. Schnellmann, *Curr. Protoc. Pharmacol.*, 2012, **56**, 12.8.
86 A. Di Rita, P. D'Acunzo, L. Simula, S. Campello, F. Strappazzon and F. Cecconi, *Front. Cell. Neurosci.*, 2018, **12**, 92.
87 H. Zhang and J. Robinson, *Drugs Pharm. Sci.*, 1996, **74**, 51–63.
88 M. J. Rathbone, *Oral Mucosal Drug Delivery*, Marcel Dekker, 1996, vol. 74.
89 J. Hao and P. W. Heng, *Drug Dev. Ind. Pharm.*, 2003, **29**, 821–832.
90 C. A. Squier and B. K. Hall, *J. Invest. Dermatol.*, 1985, **84**, 176–179.
91 V. Davenport, E. Groves, R. E. Horton, C. G. Hobbs, T. Guthrie, J. Findlow, R. Borrow, L. M. Næss, P. Oster, R. S. Heyderman and N. A. Williams, *J. Infect. Dis.*, 2008, **198**, 731–740.
92 T. Pniewski, J. Kapusta, P. Bociag, J. Wojciechowicz, A. Kostrzak, M. Gdula, O. Fedorowicz-Strońska, P. Wójcik, H. Otta, S. Samardakiewicz, B. Wolko and A. Płucienniczak, *J. Appl. Genet.*, 2011, **52**, 125–136.

